Energy & Environmental Science

Accepted Manuscript

ROYAL SOCIETY OF CHEMISTRY

www.rsc.org/ees

Journal Name

COMMUNICATION

High efficiency methylammonium lead triiodide perovskite solar cells: the relevance of non-stoichiometric precursors

Received 00th January 20xx,
Accepted 00th January 20xx

DOI: 10.1039/x0xx00000x

www.rsc.org/

C. Roldán-Carmona,[a†] P. Gratia,[a†] I. Zimmermann,[a†] G. Grancini,[a] P. Gao,[a] M. Graetzel[b] and Mohammad Khaja Nazeeruddin[a]

Methylammonium lead iodide perovskite solar cells with improved performance and stability have been succesfully prepared by using a non-stoichiometric PbI_2 : CH_3NH_3I ratio in the precursor solution, which yield power conversion efficiency (PCE) of above 19% under 1 sun for the champion cell.

In the past few years, organic-inorganic metal halide perovskite compounds became one of the best photovoltaic materials for solution-processed high efficient thin-film solar cells. Since the first report on perovskite solar cells (PSC) by *Kojima et al.,*[1] tremendous efforts have been made in understanding and controlling the growth of these hybrid materials and their optoelectronic properties.[2-7] Most of the reported perovskite solar cells in the literature are based on methylammonium lead iodide perovskite $CH_3NH_3PbI_3$, with spiro-OMeTAD as a hole-transporting material exhibiting PCE values over 17 %.[8-11] The methylammonium lead iodide perovskite ($APbX_3$) bandgap has also been tuned by substituting the organic cation (A) and the halide anions (X) on the $APbX_3$ structure, evidencing their remarkable influence in the stability and optoelectronic properties of the resulting photoactive materials.[12] Following this strategy several studies have been successfully reported using mixed halide perovskites, which focus mainly on the exchange of I^- through Br^- in the $CH_3NH_3PbI_3$ structure, resulting in the solid solution $(CH_3NH_3Pb(I_{1-x}Br_x)_3$ with $0 < x < 1$). However these devices exhibit power conversion efficiencies below those reported for the pristine material.[13,14] Mixed halide precursor solutions containing I^- and Cl^- ions were also used since the initial stages of the field, leading to the commonly referred $CH_3NH_3PbI_{3-x}Cl_x$ perovskite. In this material the role of Cl^- ions in the final structure remains still unclear, even though it seems to enhance the charge transport[3] and to reduce the charge recombination in the device. [15,16] Nevertheless the most impressive compositional modification on the perovskite structure was pioneered by Pellet *et al.*,[17] and have been recently improved by *Jeon et al*. [18] based on a combination of formamidinium iodide (FAI) and Br^- ions with the final formula $(FAPbI_3)_{0.85}(MAPbBr_3)_{0.15}$. The results show tremendous sensitivity of the ionic composition on the final performance,[19] which is strongly influenced by the molar ratio between FAI : PbI_2 precursors. As a result, a certified PCE of 20.1 % and a noticeably low hysteresis when scanning in forward and reverse bias has been reported.[20]

In attempting to reach high efficiency, factors affecting the crystallization behaviour of the final film, deposition method, and additives are under an intense study. Focusing on the perovskite film composition, several strategies have been applied to enhance the nucleation and uniform growth of the crystalline layer.[2,9,15,21-28] The solvent engineering method[14,29] or the antisolvent vapor-assisted crystallization approach[30] are some examples where high quality perovskite films were obtained thanks to a controlled film deposition. Such a rapid development on different processing methods, as well as the interface manipulation to decrease carrier recombination, have recently boosted the power conversion efficiencies for $CH_3NH_3PbI_{3-x}Cl_x$ and $CH_3NH_3PbI_3$ perovskites to values above 19%[10,31] being comparable to the FAI based analogue,[32] a persistent caveat being the poor stability of these high efficiency devices. [31]

[a] Group for Molecular Engineering of Functional Materials, [b]Laboratory of Photonics and interfaces, Institute of Chemical Sciences and Engineering, Ecole polytechnique fédérale de Lausanne, CH-1951 Sion, Switzerland
† Those authors contributed equally to this work.
* Corresponding author. Email: mdkhaja.nazeeruddin@epfl.ch
Electronic Supplementary Information (ESI) available: [details of any supplementary information available should be included here]. See DOI: 10.1039/x0xx00000x

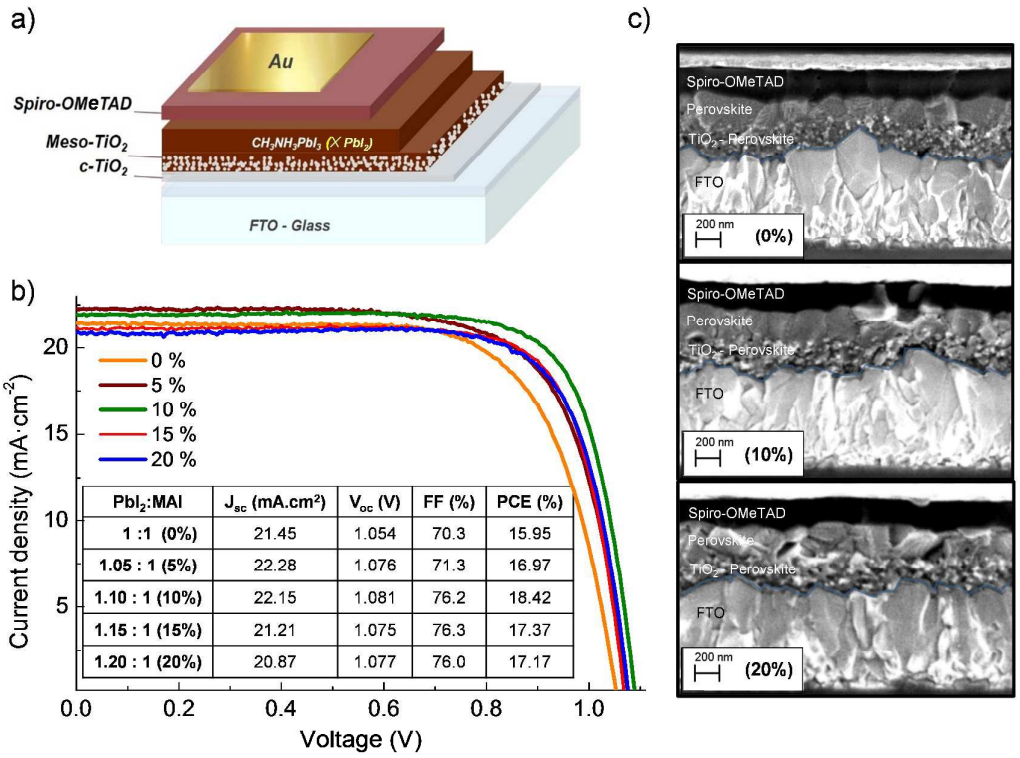

PbI_2:MAI	J_{sc} (mA.cm²)	V_{oc} (V)	FF (%)	PCE (%)
1 :1 (0%)	21.45	1.054	70.3	15.95
1.05 : 1 (5%)	22.28	1.076	71.3	16.97
1.10 : 1 (10%)	22.15	1.081	76.2	18.42
1.15 : 1 (15%)	21.21	1.075	76.3	17.37
1.20 : 1 (20%)	20.87	1.077	76.0	17.17

Fig. 1. (a) Diagram showing the device architecture used in our study, where $CH_3NH_3PbI_3$: X PbI_2 represents the active film with different stoichiometric ratios between precursors. (b) *Current density – Voltage* ($J-V$) curves obtained for the devices containing 0 – 5 – 10 – 15 – 20 % of PbI_2 molar excess in the perovskite layer measured under AM1.5G solar irradiation of 100 mW cm^{-2} and scan-rate fixed at 10 mV·s^{-1}. No stabilization time under light soaking and positive bias applied before the measurements. (c) Cross-sectional SEM of the devices. From the top to the bottom: reference cell, 10 % and 20 % molar excess samples.

In this communication we present high efficient methylammonium lead iodide perovskite solar cells in which a non-stoichiometric ratio between PbI_2 and MAI precursors (x : 1, being x ≥ 1) has been used. Due to its higher band-gap ($E_g = 2.3\ eV$), the presence of PbI_2 in the perovskite film has been considered harmful to the device performance. This may be true when its formation is associated to the perovskite degradation, such as an excessive annealing time or temperature, leading to a deterioration of the photovoltaic device. However in this study we demonstrate the influence of unreacted PbI_2 when it is incorporated as an additive in the perovskite solution. Our results demonstrate that an excess of PbI_2 improves the average fill factor (FF) and open circuit voltage (V_{oc}), boosting the averaged power conversion efficiency from 16.2 % to values close to 18 %, and an efficiency peak of above 19 % for the champion cell. These results provide another evidence that tuning PbI_2 in PSC can be an easy and effective approach towards a competitive photovoltaic alternative.[33-37]

The solar cells were fabricated on FTO covered glass substrates based on a previously reported architecture, where the active layer is sandwiched between a mesoporous TiO_2 electron transport material and 2,2'7,7'-tetrakis(N,N-di-p-methoxyphenylamine)-9,9'-spirobifluorene) (spiro-OMeTAD) hole transport layer. After cleaning the substrates by ultrasonic and UV-ozone treatment, a thin TiO_2 compact layer of 25 nm was deposited on FTO via spray pyrolysis at 450°C, followed by a sintering process of the layer at 450 °C during 30 minutes. Then a mesoporous TiO_2 layer was deposited by spin coating a 30 nm particle paste (Dyesol 30 NR-D) diluted in ethanol for 10 s at 4000 rpm, to achieve 150 nm thick layer. These layers were sintered again at 450°C for 30 min under dry air flow. For further details about the substrate and TiO_2 preparation see Supporting Information. The perovskite films were prepared from a precursor solution 1.25 M of both components PbI_2 and CH_3NH_3I in dimethyl sulfoxide (DMSO) in the case of 1:1 molar ratio. Different compositions with 5 – 10 – 15 – 20 % molar excess of PbI_2 were also tested by fixing the MAI concentration in the precursor solution and adjusting the amount of PbI_2. The perovskite solution was then deposited by a previously reported method[38] with slight modifications on the deposition process, as it is described in the Supporting Information. This process consist of the deposition of the precursor solution followed by chlorobenzene drop-casting in

a similar way as the solvent engineering method previously reported.[29] The resulted film was uncoloured and transparent, indicating the formation of a smooth film of the CH_3NH_3I–PbI_2–DMSO intermediate phase. This film was then annealed at 100°C during 45 minutes in an inert atmosphere to favour a good crystallization of the perovskite layer. Finally, a 200 nm layer of doped spiro-OMeTAD was deposited as the hole transport material prior to the deposition of 100 nm gold as the electrode. Figure 1a shows the device architecture of the studied perovskite solar cells.

Figure 1b shows the $J-V$ curves recorded under standard AM1.5G solar spectrum illumination conditions obtained for devices containing perovskite active layers with different composition, where an excess of lead iodide have been added intentionality in the solution. In order to demonstrate the influence that using a non-stoichiometric ratio generates in the device performance, five different perovskite solutions with molar excess of lead iodide among 0 – 20 % have been tested. The most representative devices, which are close to the averaged results obtained for each condition are shown in Figure1b, with the main device parameters summarized in the inset table. As it is observed in the figure, all perovskite solar cells exhibit excellent performances even when an excess of PbI_2 as high as 20 % is incorporated in the active layer, obtaining the maximum power conversion efficiency for concentrations with 10 % excess of PbI_2 respect to the stoichiometric ratio. Compared to the reference cell, where a ratio PbI_2 : MAI (1 : 1) has been used, the short circuit current density J_{sc} increases slightly with the presence of PbI_2 in the film, leading to its maximum improvement for perovskite films containing between 5 – 10 % PbI_2 molar excess. A similar trend is observed in the open circuit voltage, V_{oc}, which improves considerably in the presence of small amounts of unreacted PbI_2, reaching an average value $\overline{V_{oc}}$ = 1.080 V for cells containing 10 % of PbI_2 excess and a maximum value as high as V_{oc} = 1.11 V for its best result. However, the device parameter which is most influenced by the presence of unreacted PbI_2 is the fill factor. All PSC containing PbI_2 : MAI (x : 1) with x ≥ 1.1 exhibit an important improvement in the fill factor, showing averaged values $\overline{FF}$ above 76 % in all cases. This influence is more pronounced when 10% of unreacted PbI_2 is present in the $CH_3NH_3PbI_3$ layer, leading to an impressive value of 80.7 % for the best result when scanning in forward bias, which appears to be the highest value reported for n-i-p structures. An even higher value of 0.85 was achieved in our recent study for p-i-n structures,[39] which is very close to the theoretical limit of 0.89.[40,41] It is worth noting that high FF values are frequently obtained for solar cells with low current densities, J, where resistive losses could be minimized. The photovoltaic performance of the champion cell, which led to an impressive power conversion efficiency of 19.1 % is shown in Figure 2. The incident photon-to-current efficiency (IPCE) (Fig. 2b) of the champion perovskite device as a function of wavelength obtained shows that the generation of photocurrent begins at ~820 nm and the photocurrents obtained from the IPCE data are in close agreement with those of current-voltage measurements. Interestingly, the prepared cells present a negligible hysteresis (see Figure S6) between forward and reverse scan in the $J-V$ curves, as well as a remarkably stability (see Figure S8), showing no significant deterioration after more than 3 months in dry air and dark conditions.

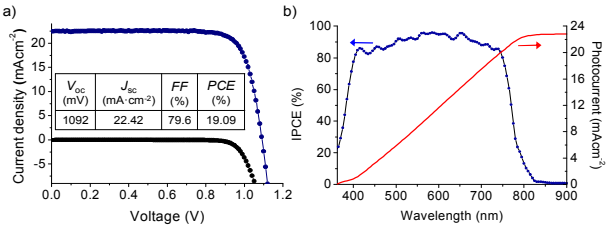

Fig. 2. (a) $J-V$ curve measured for the champion cell under AM 1.5G illumination in ambient atmosphere. The cell was measured without encapsulation at a constant rate 100 mV·s^{-1}. b) IPCE spectrum obtained for the champion cell (blue line) and integrated photocurrent that is expected to be generated under AM 1.5G irradiation (red line).

In order to achieve a deeper understanding of the origin of such high performances further investigations concerning surface characterization and spectroscopy measurements were recorded for all the perovskite films. Figure 1c shows the cross-sectional scanning electron microscopy (SEM) view of the perovskite solar cells containing 10 % and 20 % excess of PbI_2, as well as the corresponding image for the reference cell. The individual layers that form the device can be easily differentiated in the images, being their composition indicated for clarity in the left legend. In all cases the perovskite layer consists of two different regions, one based on an infiltrated perovskite through a 150 nm mesoscopic TiO_2-film capped with a solid perovskite layer with ~ 200 nm thickness. Although the images are similar, there is a noticeable change in morphology in the perovskite capping layers as the unreacted excess of PbI_2 increases. As can be observed, the stoichiometric perovskite film exhibits a granulated capping layer where the grain crystals are not well defined. As the amount of PbI_2 in the perovskite material increases, larger and more homogeneous defined grain-crystals are formed. This change could be attributed to a better crystallization of the perovskite layer, which leads to larger crystals in the capping layer in presence of excess of PbI_2. For clarity only 3 different compositions are shown in Figure 3b. The SEM images corresponding to the rest of the studied stoichiometries are shown in Figure S1, as well as the grain-size distribution obtained for each composition.

To further investigate the role of PbI_2 in the crystallization process of the perovskite material, X-ray diffraction (XRD) experiments have been performed for the different films, with 0 – 30 % excess of PbI_2 in the photoactive layer. Figure 3a shows the diffractograms obtained for the different $CH_3NH_3PbI_3$: *x* PbI_2 compositions. The X-ray patterns confirm the presence of the tetragonal perovskite phase of $CH_3NH_3PbI_3$ in all of the prepared films. As previously reported, the excess of lead iodide can be monitored looking at the characteristic

PbI_2 peak located at 2θ of around 12.7°. Very little unreacted lead iodide can be seen for the film prepared using a stoichiometric mixture of the starting materials. This indicates a close to complete conversion into the perovskite phase. As expected, the increasing excess of lead iodide ranging from 5 – 30 % can be clearly observed in the diffraction patterns.

Interestingly, an increasing amount of PbI_2 in the films also results in more intense perovskite peaks. The inset in the figure shows how the intensity of the (110) peak from the perovskite increases with excess of lead iodide. This phenomenon can be explained by an increased film thickness, a more dense packing of the perovskite grains or an increased crystallinity within the thin films. From SEM cross-section images no significant change in the thickness of the perovskite film could be observed. This is a strong indication for an overall improvement of the quality of the perovskite films within the device with the presence of unreacted lead iodide. Looking at the peak shape, a decrease in the peak broadening can be also observed with the excess of lead iodide, which can be associated with a larger size of the perovskite grains within the capping layer of the films (the values for the full width at half maximum (FWHM) are also indicated in the inset). SEM images obtained from the surface analysis of the perovskite films are also shown in Figure 3b, which confirm the variation on the grain-size with the film composition.

As will be confirmed by the optical analysis shown below, the formation of larger crystals can be intrinsically related to a more relaxed lattice structure formed during the crystallization process in the presence of PbI_2 excess.[50, 52] It has been demonstrated in literature[50, 52] that the interplay between organic and inorganic interactions affects the lattice strain, influencing the band gap of the semiconductors. If the organic cations freeze in a preferential head-to-tail-like configuration, the lattice strain is reduced and the $CH_3NH_3PbI_3$ tends to crystallize into larger grains. The reduced strain leads to a lattice expansion, resulting in a reduced bandgap observed as a red shift in the photoluminescence emission.[50, 52] From one side, in our work we have evidence from the SEM measurements of the larger crystal domains of the capping layer obtained in the presence excess of PbI_2. On the other side, the corresponding photoluminescence spectra show a red shift of the emission (see spectral shift of the normalized curves in Figure 4b), indicative of a reduced band gap associated to the improved crystallization.

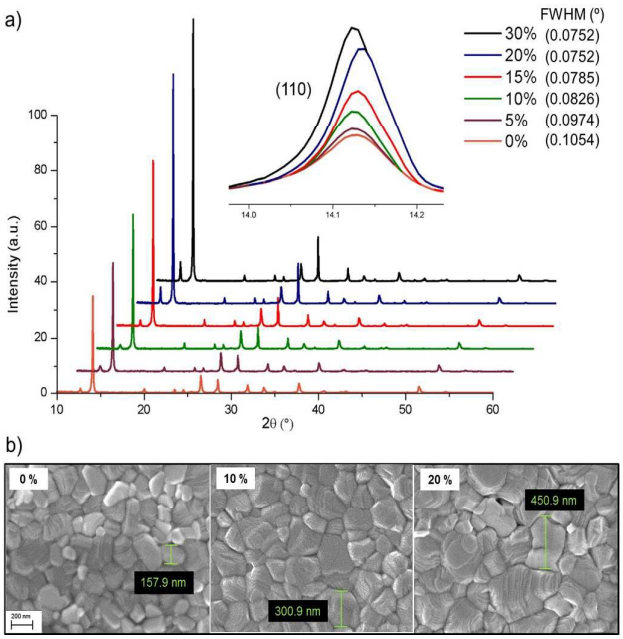

Fig. 3. a) XRD patterns of the different perovskite films with each composition indicated in the legend. The Inset shows the magnified graph in the 2θ range of 14° – 14.3° corresponding to the characteristic peak (110) on the perovskite structure as well as the FWHM values. b) SEM pictures corresponding to the surface analysis of the films.

In order to understand the difference between the perovskite crystals we further characterized the films by using optical steady state (UV-vis, Photoluminescence (PL)) along with time resolved PL spectroscopy. Figure 4 shows the absorption and PL spectra of the different perovskite layers prepared with 0 – 20 % PbI_2 excess. Due to the high absorption coefficient of the perovskite material at high frequencies, only the absorption spectra in the visible region λ > 400 nm is shown (see Figure 4a). Similar absorption onset centered at ~ 770 nm are obtained for all the films, exhibiting small differences in their absorption intensities. The films prepared with a stoichiometric ratio of both precursors had the highest absorption, which decreases for the rest of the films proportionally to the PbI_2 content. This can be related with a lower concentration of $CH_3NH_3PbI_3$ material present in the film due to the limited CH_3NH_3I content in the precursor solution. When high quality perovskite films are formed through improved crystallization, factors such as charge dissociation efficiency, charge transport and diffusion length of charge species are the main affected parameters. Previous studies on perovskite devices have demonstrated that a non-radiative trap-assisted recombination takes place in the perovskite films, which represents a loss in the generated free carriers and thus in power conversion efficiency.[33,42-46] Time resolved photoluminescence (TRPL) spectroscopy have been recently used to obtain important information about perovskite film quality, with longer carrier recombination lifetimes (τ) indirectly indicating longer charge diffusion length[3,47] and superior performance.[27,48,49]

Here we perform TRPL spectroscopic investigation to gain a deeper understanding on the influence of the excess PbI_2 in the fundamental photo-induced dynamical processes. It is worth mentioning that, given the high absorption coefficient of the perovskite, the light penetration depth at 460 nm can be estimated in the 50-100 nm range.[50] Therefore, as one can observe from the inset of Figure 4c, due to the asymmetric nature of the perovskite device configuration, the excitation from the TiO_2 substrate side (scaffold thickness ~ 150 nm) will exclusively interrogate the physical properties of the perovskite nano-crystallites grown within the oxide scaffold, on the other hand, excitation from the capping layer side (~ 150 nm thick) will only probe the intrinsic processes of the large perovskite grains. This will enable us to disentangle the effects due to the excess of PbI_2 content on the intrinsic properties of the perovskite capping layer from the ones induced at the active perovskite/TiO_2 interface.

Figure 4b shows the PL spectra as well as the normalized data for the two limiting conditions: 0 % and 20 % PbI_2 excess. Typical sharp PL spectra with very little Stokes-shift centered at ~ 770 nm are also observed for all cases, which is in agreement with the previously reported data in the literature.[3] The PL spectra and dynamics in Figure 4b and right panel of Figure 4d, respectively, have been measured from the capping layer side. We observe a trend when increasing the content of the unreacted PbI_2 in terms of: *i)* higher PL intensities (that reaches a maximum value for the 15 %–excess sample) than the stoichiometric $CH_3NH_3PbI_3$ films; *ii)* a continuous red-shift of the PL peak (normalized data relative to the reference and the 20 %–excess samples show a displacement of 10 nm in their maximum emission wavelength) and *iii) a* longer-living PL component exceeding out temporal window of 100 ns (Figure 4d, right panel). Overall, these observations suggest that the crystallization dynamics dramatically impact on the photophysical scenario. Similar trends have been previously reported by some groups[50-52] who found that morphological changes (i.e. dimension of crystal grains) affect the optical properties of the perovskite films: tuning the average crystallite dimension changes the optical band gap of the material along with its photoluminescence lifetime. In particular, larger crystallites present a smaller band gap (i.e. red-shifted PL as we do observe) and longer lifetime, which correlates to a smaller radiative bimolecular recombination coefficient.[50] DeQuilettes *et al.*,[53] also reported a strong quenching in the PL spectra caused by the presence of defect states or shallow trapping levels in the grain boundaries of the perovskite, which frequently behave as non-radiative recombination centres. Similar effect is induced in our case by the presence of the excess of PbI_2. The observed shrinkage of the optical band gap along with the enhance PL lifetime support the formation of larger perovskite crystal grains (consistent with our results from the X-Ray diffraction patterns analysis) that can be mainly due to a change in the local order of the crystalline structure.[12,50,52]

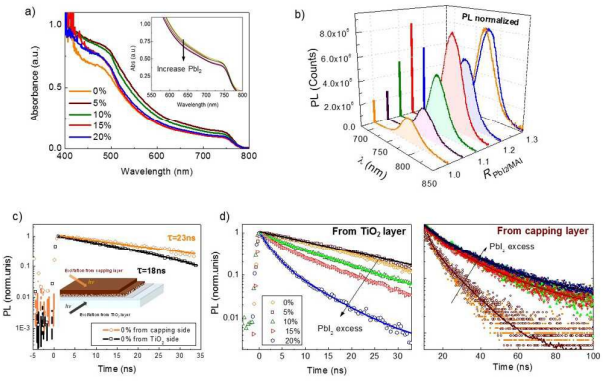

Fig. 4. (a) Normalized UV-Vis absorption spectra measured for the perovskite films containing different amounts of PbI_2. The inset shows the non-normalized spectra in the region between 550 – 800 nm, where the arrow indicates the increase of PbI_2 in the samples. (b) 3-D graph with the evolution of the steady state photoluminescence spectra with the perovskite compositions ($R_{PbI2/MAI}$) at an excitation wavelength λ_{exc} = 600 nm. The projections in the PL - $R_{PbI2/MAI}$ and PL – λ planes show the evolution of the signal intensity and maximum emission wavelength when the amount of PbI_2 increases. (c) Time resolved photoluminescence decay at 770 nm obtained for the reference cell and for the non-stoichiometric films upon excitation at λ_{exc} = 460 nm, excitation density of ~10 mW/cm^2 (d) at 770 nm The samples were excited from both the perovskite capping layer and from the TiO_2 side. The samples were all encapsulated to prevent any degradation or oxygen effects during the measurements.

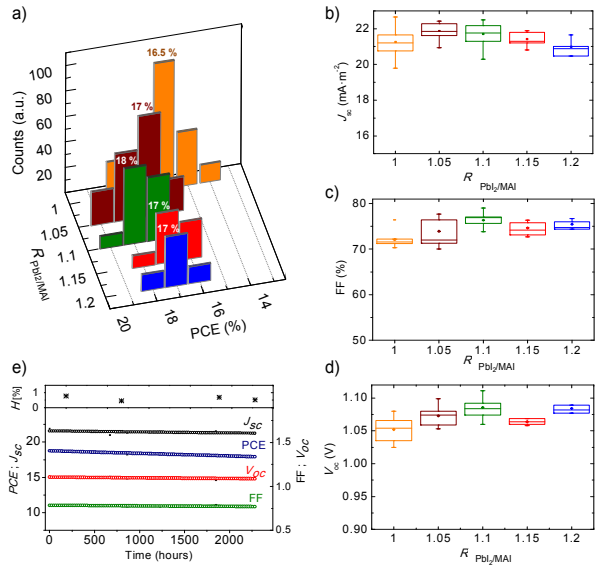

Fig. 5. (a) Histogram of PSC efficiencies for more than 50 devices with the configuration FTO/c-TiO_2/m-TiO_2/(Perovskite: X PbI_2)/Spiro-OMeTAD/Au, where X corresponds to different PbI_2 molar excess. The average values of the photovoltaic parameters $\overline{J_{sc}}$, $\overline{FF}$ and $\overline{V_{oc}}$ for those devices are also shown in the figures (b), (c) and (d) respectively. (e) Evolution of the photovoltaic parameters of one of our record cells after more than 2.500 hours ($J_{sc}(0) = 21.9\, mA \cdot cm^{-2}$; $V_{oc}(0)$ = 1.103 V; $FF(0)$ = 78.7 %; $PCE(0)$ = 18.81 %). The inset includes the absolute hysteresis H (%) = PCE_{rev} - PCE_{fow} observed when the cell is

scanned in forward or reverse bias, which is lower than 0.8 % in all cases.

To get a comprehensive picture on the influence of the excess of PbI_2 amount on device physics we also excited the device from the mesoporous TiO_2 layer, in order to analyze the perovskite/TiO_2 interface. Figure 4c shows the PL decay of the reference sample from both excitation sides: when the light is shined from the TiO_2 side we observe a slight quenching of the PL decay with respect to what is obtained upon the capping layer excitation. It is true that small crystals confined in an insulating mesoporous oxide structure generally exhibit faster PL dynamics due to their intrinsic shorter charge recombination lifetime[51] however, this usually happens in the hundreds of nanoseconds time window. The much faster quenching that we observe is more reasonably attributed to the more efficient charge extraction happening at the conductive TiO_2 interface, where electron injection occurs, thus reducing the PL lifetime. Figure 4c left panel shows the PL decay obtained for the studied samples when the excitation takes place through the TiO_2-meso side. A clear trend can be observed in the TRPL response of the perovskite with the presence of unreacted PbI_2. When increasing PbI_2 content the PL shows a faster decay component (with a time constant down to 2 ns for the 20 % sample, see TableS1 in Supporting Information). This observation indicates that the excess of PbI_2 leads to faster PL quenching indicative of a more efficient electron transfer to TiO_2. We infer that this effect might be induced both by a better energy level alignment and stronger interfacial coupling at the interface as recently theoretically predicted for the mixed-halide perovskite,[54] enhancing the charge extraction, or by a beneficial passivation effect of the iodine atoms at the interface.

Figure 5a-d summarizes the photovoltaic parameters obtained from more than 50 devices, where the improvement due to unreacted PbI_2 is clearly observed. For clarity in the figure, the peak intensity of each histogram have been adjusted for the different $R_{PbI2/MAI}$ ratios. The numbers on the diagram indicates the PCE value for the most populated segment, which correlates with the averaged $\overline{PCE}$ value obtain for each composition. The averaged values for the rest of photovoltaic parameters are also reported in Figure 4b-d, where a clear enhancement is observed for $R_{PbI2/MAI} \approx 1.1$. Our results demonstrate that the quality of $CH_3NH_3PbI_3$ films can be easily enhanced without many modifications with respect to the reported device architectures by adding an excess of PbI_2 precursor in the perovskite film. The unreacted PbI_2 may enhance the crystallinity and reduce the non-radiate recombination pathways at the perovskite interface, leading to an impressive improvement in the photovoltaic performance compared with the reference material. With this approach, methylammonium lead iodide perovskite solar cells with higher reproducibility and improved stability can be obtained. As a remark, a first stability evaluation for one of our record cells is also shown in Figure 5b (for comparison with the reference cell see also Figure S9). The cell, which was stored in dry air without any encapsulation, did not deteriorate after more than 2.500 hours after its preparation, remaining with a PCE hysteresis lower than 0.8 % during this time.

Conclusions

We have successfully prepared high efficient methylammonium lead iodide perovskite solar cells by incorporating an excess of PbI_2 as an additive in the film. Our results suggest that the unreacted PbI_2 improves the crystallinity of the perovskite film and the electron transfer to the TiO_2 layer, both leading to the impressive improved performances even for a molar excess of 20%. This provides an evidence of the unnecessary use of a stoichiometric ratio between PbI_2 : MAI precursors, as has been commonly thought in the field, and represent an effective approach for boosting the efficiency closer to its theoretical value.

Acknowledgments

This work was supported by the European Union Seventh Framework Programme [FP7/2007-2013] under grant agreement n° 604032 of the MESO project, (FP7/2007-2013) ENERGY.2012.10.2.1; NANOMATCELL, grant agreement no. 308997, and H2020-ICT-2014-1, grant agreement N°: 643791. We thank Drs. J.-P Correa Baena (LPMS, EPFL), Antonio Abate and Fabrizio Giordano (LPI,EPFL) for providing the initial recipe for the fabrication of the perovskite solar cells.

Notes and references

(1) A. Kojima, K. Teshima, Y. Shirai and T. Miyasaka, *JACS* 2009, ***131***, 6050.
(2) M. M. Lee, J. Teuscher, T. Miyasaka, T. N. Murakami and H. J. Snaith, *Sci.* 2012, ***338***, 643.
(3) S. D. Stranks, G. E. Eperon, G. Grancini, C. Menelaou, M. J. P. Alcocer, T. Leijtens, L. M. Herz, A. Petrozza, H. J. Snaith, *Sci.* 2013, ***342***, 341.
(4) J. M. Frost, K. T. Butler, F. Brivio, C. H. Hendon, M. van Schilfgaarde and A. Walsh, *Nano Lett.* 2014, ***14***, 2584.
(5) G. Xing, N. Mathews, S. Sun, S. S. Lim, Y. M. Lam, M. Graetzel, S. Mhaisalkar and T. C. Sum, *Sci.* 2013, ***342***, 344.
(6) W.Tress, N. Marinova, T. Moehl, S. M. Zakeeruddin, M. K. Nazeeruddin and M. Graetzel, *Energy Environ. Sci.* 2015, ***8***, 995.
(7) H.-S. Kim, C.-R. Lee, J.-H. Im, K.-B. Lee, T. Moehl, A. Marchioro, S.-J. Moon, R. Humphry-Baker, J.-H. Yum, J. E. Moser, M. Graetzel and N.-G. Park, *Sci. Rep.*2012, ***2***, 1.
(8) Z. Xiao, C. Bi, Y. Shao, Q. Dong, Q. Wang, Y. Yuan, C. Wang, Y. Gao and J. Huang, *Energy Environ. Sci* 2014, ***7***, 2619.
(9) Q. Chen, H. Zhou, Z. Hong, S. Luo, H.-S. Duan, H.-H. Wang, Y. Liu, G. Li and Y. Yang, *JACS* 2014, ***136***, 622.
(10) N. Ahn, D.-Y. Son, I.-H. Jang, S. M. Kang, M. Choi, N.-G. Park, *JACS* 2015, ***137***, 8696.
(11) J.-H. Im, I.-H. Jang, N. Pellet, M. Graetzel and N.-G. Park, *Nat. Nanotechnol.* 2014, ***9***, 927.

(12) E. Mosconi, A. Amat, M. K. Nazeeruddin, M. Graetzel and F. De Angelis, *J. Phys. Chem. C* 2013, ***117***, 13902.
(13) S. A. Kulkarni, T. Baikie, P. P. Boix, N. Yantara, N. Mathews, S. Mhaisalkar, *J. Mat. Chem. A* 2014, ***2***, 9221.
(14) J. H. Heo, D. H. Song and S. H. Im, *Adv. Mater.* 2014, ***26***, 8179.
(15) M. Liu, M. B. Johnston, H. J. Snaith, *Nature* 2013, ***501***, 395.
(16) P. Delugas, A. Filippetti and A. Mattoni, *Phys. Rev.B* 2015, ***92***.
(17) N. Pellet, P. Gao, G. Gregori, T.-Y. Yang, M. K. Nazeeruddin, J. Maier and M. Graetzel, *Angew. Chem. Int. Edit.* 2014, **53**, 3151.
(18) N. J. Jeon, J. H. Noh, W. S. Yang, Y. C. Kim, S. Ryu, J. Seo, S. I. Seok, *Nature* 2015, ***517***, 476.
(19) S. Pang, H. Hu, J. Zhang, S. Lv, Y. Yu, F. Wei, T. Qin, H. Xu, Z. Liu and G. Cui, *Chem. Mater.* 2014, ***26***, 1485.
(20) NREL Best Research-Cell Efficiencies, 2015.
(21) J. Burschka, N. Pellet, S.-J. Moon, R. Humphry-Baker, P. Gao, M. K. Nazeeruddin and M. Graetzel, *Nature* 2013, ***499***, 316.
(22) J.-Y. Jeng, Y.-F. Chiang, M.-H. Lee, S.-R. Peng, T.-F. Guo, P. Chen and T.-C. Wen, *Adv. Mater.*2013, ***25***, 3727.
(23) D. Liu, T. L. Kelly, *Nat. Photonics* 2014, ***8***, 133.
(24) O. Malinkiewicz, C. Roldán-Carmona, A. Soriano, E. Bandiello, L. Camacho, M. K. Nazeeruddin, H. J. Bolink, *Adv. Energy Mat.*2014, *4*.
(25) G. E. Eperon, V. M. Burlakov, P. Docampo,; A. Goriely and H. J. Snaith, *Adv. Funct. Mater.*2014, ***24***, 151.
(26) G. Longo, L. Gil-Escrig, M. J. Degen,; M. Sessolo and H. J. Bolink, *Chem. Commun.* 2015, ***51***, 7376.
(27) P. W. Liang, C. Y. Liao, C. C. Chueh, F. Zuo, S. T. Williams, X. K. Xin, J. J. Lin and A. K. Y. Jen, *Adv. Mater.* 2014, ***26***, 3748.
(28) D. Forgacs, M. Sessolo and H. J. Bolink, *J. Mat. Chem. A* 2015, ***3***, 14121.
(29) N. J. Jeon, J. H. Noh, Y. C. Kim, W. S. Yang, S. Ryu, S. Il Seol, *Nat. Mater.* 2014, ***13***, 897.
(30) D. Shi, V. Adinolfi, R. Comin, M. Yuan, E. Alarousu, A. Buin, Y. Chen, S. Hoogland, A. Rothenberger, K. Katsiev, Y. Losovyj, X. Zhang, P. A. Dowben, O. F. Mohammed, E. H. Sargent and O. M. Bakr, *Sci.* 2015, ***347***, 519.
(31) H. Zhou, Q. Chen, G. Li, S. Luo, T.-b. Song, H.-S. Duan, Z. Hong, J. You, Y. Liu, Y. Yang, *Sci.* 2014, ***345***, 542.
(32) W. S. Yang, J. H. Noh,; N. J. Jeon, Y. C. Kim, S. Ryu, J. Seo and S. I. Seok, *Sci.* 2015, ***348***, 1234.
(33) L. Wang, C. McCleese, A. Kovalsky, Y. Zhao and C. Burda, *JACS* 2014, ***136***, 12205.
(34) T. Salim, S. Sun, Y. Abe, A. Krishna, A. C. Grimsdale and Y. M. Lam, *J. Mat. Chem. A* 2015, ***3***, 8943.
(35) Y. H. Lee, J. Luo, R. Humphry-Baker, P. Gao, M. Graetzel and M. K. Nazeeruddin, *Adv. Funct. Mater.* 2015, ***25***, 3925.
(36) Q. Chen, H. Zhou, T.-B. Song, S. Luo, Z. Hong, H.-S. Duan, L. Dou, Y. Liu, Y. Yang, *Nano Lett.* 2014, ***14***, 4158.
(37) T. Supasai, N. Rujisamphan, K. Ullrich, A. Chemseddine, T. Dittrich, *Appl. Phys. Lett.*2013, ***103***.
(38) A. Abate, S. Paek, F. Giordano, J.-P. Correa-Baena, M. Saliba, P. Gao, T. Matsui, J. Ko, S. M. Zakeeruddin, K. H. Dahmen, A. Hagfeldt, M. Grätzel, M. K. Nazeeruddin, *Energy Environ. Sci* 2015, *10.1039/C5EE02014J*.
(39) C.-G. Wu, C.-H. Chiang, Z.-L. Tseng, M. K. Nazeeruddin, A. Hagfeldt and M. Grätzel, *Energy Environ. Sci* 2015, *DOI: 10.1039/c5ee00645g*.
(40) M.A. Green, S. C., Prentice-Hall, Englewood Cliffs, NJ, 1982, p. 88.
(41) P. Singh and N. M. Ravindra, *Sol. Energy Mater. Sol. Cells* 2012, ***101***, 36.
(42) Y. Yamada, T. Nakamura, M. Endo, A. Wakamiya, Y. Kanemitsu, *JACS* 2014, ***136***, 11610.
(43) S. D. Stranks, V. M. Burlakov, T. Leijtens, J. M. Ball, A. Goriely and H. J. Snaith, *Phys. Rev. Appl.* 2014, ***2***.
(44) G.-J. A. H. Wetzelaer, M. Scheepers, A. Miquel Sempere, C. Momblona, J. Avila and H. J. Bolink, *Adv. Mater.*2015, ***27***, 1837.
(45) W. Tress, N. Marinova, O. Inganas, M. K. Nazeeruddin, S. M. Zakeeruddin and M. Graetzel, *Adv. Energy Mat.* 2015, ***5***.
(46) N. Marinova, W. Tress, R. Humphry-Baker, M. I. Dar, V. Bojinov, S. M. Zakeeruddin, M. K. Nazeeruddin and M. Graetzel, *Acs Nano* 2015, ***9***, 4200.
(47) H. J. Snaith, *J. Phys. Chem. Lett.* 2013, ***4***, 3623.
(48) N. K. Noel, A. Abate, S. D. Stranks, E. S. Parrott, V. M. Burlakov, A. Goriely and H. J. Snaith, *Acs Nano* 2014, ***8***, 9815.
(49) J. You, Z. Hong, Y. Yang, Q. Chen, M. Cai, T.-B. Song, C.-C. Chen, S. Lu, Y. Liu, H. Zhou and Y. Yang, *Acs Nano* 2014, ***8***, 1674.
(50) V. D'Innocenzo, A. R. Srimath Kandada, M. De Bastiani, M. Gandini and A. Petrozza, *JACS* 2014, ***136***, 17730.
(51) M. De Bastiani, V. D'Innocenzo, S. D. Stranks, H. J. Snaith and A. Petrozza, *Apl Materials* 2014, ***2***.
(52) G. Grancini, S. Marras, M. Prato, C. Giannini, C. Quarti, F. De Angelis, M. De Bastiani, G. E. Eperon, H. J. Snaith, L. Manna, A. Petrozza, *The J. Phys. Chem. Lett.* 2014, ***5***, 3836.
(53) D. W. deQuilettes, S. M. Vorpahl, S. D. Stranks, H. Nagaoka, G. E. Eperon, M. E. Ziffer, H. J. Snaith and D. S. Ginger, *Sci.* 2015, ***348***, 683.
(54) E. Mosconi, E. Ronca and F. De Angelis, *J. Phys. Chem. Lett.* 2014, ***5***, 2619.